# Density functional theory and simulations of colloidal triangular prisms

Matthieu Marechal, Simone Dussi, and Marjolein Dijkstra

Citation: The Journal of Chemical Physics **146**, 124905 (2017); doi: 10.1063/1.4978502
View online: http://dx.doi.org/10.1063/1.4978502
View Table of Contents: http://aip.scitation.org/toc/jcp/146/12
Published by the American Institute of Physics

**Articles you may be interested in**

A molecular Debye-Hückel theory and its applications to electrolyte solutions: The size asymmetric case
The Journal of Chemical Physics **146**, 124118124118 (2017); 10.1063/1.4978895

Langevin-Poisson-EQT: A dipolar solvent based quasi-continuum approach for electric double layers
The Journal of Chemical Physics **146**, 044108044108 (2017); 10.1063/1.4973934

Phase behaviour of quasicrystal forming systems of core-corona particles
The Journal of Chemical Physics **146**, 114901114901 (2017); 10.1063/1.4977934

# Density functional theory and simulations of colloidal triangular prisms

Matthieu Marechal,[1,a)] Simone Dussi,[2,a)] and Marjolein Dijkstra[2]
[1]*Institut für Theoretische Physik, Universität Erlangen-Nürnberg, Staudtstr. 7, 91058 Erlangen, Germany*
[2]*Soft Condensed Matter, Debye Institute for Nanomaterials Science, Utrecht University, Princetonplein 5, 3584 CC Utrecht, The Netherlands*

(Received 3 January 2017; accepted 24 February 2017; published online 31 March 2017)

Nanopolyhedra form a versatile toolbox to investigate the effect of particle shape on self-assembly. Here we consider rod-like triangular prisms to gauge the effect of the cross section of the rods on liquid crystal phase behavior. We also take this opportunity to implement and test a previously proposed version of fundamental measure density functional theory (0D-FMT). Additionally, we perform Monte Carlo computer simulations and we employ a simpler Onsager theory with a Parsons-Lee correction. Surprisingly and disappointingly, 0D-FMT does not perform better than the Tarazona and Rosenfeld's version of fundamental measure theory (TR-FMT). Both versions of FMT perform somewhat better than the Parsons-Lee theory. In addition, we find that the stability regime of the smectic phase is larger for triangular prisms than for spherocylinders and square prisms. *Published by AIP Publishing.* [http://dx.doi.org/10.1063/1.4978502]

## I. INTRODUCTION

Recent advances in colloid synthesis techniques allow the preparation of colloids and nanoparticles with a larger number of distinct polyhedral shapes and sizes ranging from the nanometer to the micrometer.[1–3] With this great variety of available polyhedral shapes, polyhedra are attractive as a toolbox for investigating the effect of shape on self-assembly.[4–9] This requires efficient theories or computer simulations to guide future synthesis efforts. In fact, a synergy of the two types of techniques could be used: First, a reliable and efficient, but approximate, theory predicts the phase behavior for a large range of parameters. Subsequently, particle-resolved computer simulations improve on these predictions at the cost of a greater computational effort.

A range of theoretical techniques exist for hard bodies: The fluid and the crystal can be described using scaled particle theory and cell theory, respectively, while the most suitable non-phenomenological theory for liquid crystals is density functional theory (DFT).[10,11] Density functional theory is a continuum theory for systems that are inhomogeneous or anisotropic either due to applied external fields[10,12,13] or spontaneous symmetry breaking.[14–16] For hard spheres, the most successful DFT is fundamental measure theory (FMT)[15,17,18] or an extension.[19–22] FMT is strongly based on geometry, which makes the extension to non-spherical particles[12,13,23,24] more elegant than for previous DFTs for anisotropic particles.[25–28] FMT has been successfully applied to polyhedra with moderate shape anisotropy.[29] More recent advances,[30,31,33] after which the smectic phase of rods can be described, were not implemented in Ref. 29.

The existence of polyhedral nanorods[3,34–36] and the observation of smectic-like ordering of these rods[34,35] motivated us to consider the effect of polyhedral shape on the liquid-crystal phases of rod-like particles. Furthermore, polyhedral rods present a good system to test the recent advances from Refs. 30–33 for shapes other than spherocylinders and to investigate the performance of a fully non-empirical version of FMT (see Sec. III) which has not yet been applied to non-spherical particles. We chose the triangular prisms as the rod-like polyhedron to consider as it is the prism that differs the most from the spherocylinder. Computer simulations of square prisms (also known as cuboids or tetragonal parallelepipeds) have already been performed[37,38] showing the expected liquid crystal phases for sufficient elongation.

This paper is organized as follows: First, we present the model and its parameters in Sec. II. In the subsequent section (Sec. III), we first present the two versions of FMT we will consider. In Sec. IV, we describe a simpler (Onsager-like) theory; the performance of the more complicated FMT will be compared to this theory for the nematic phase. Sec. VI contains our results. Finally, we will summarize our results in Sec. VII and compare them to results for other particles shapes. The appendices contain details considering the implementation of FMT for general shapes (in Appendix A) and the specialization to polyhedra (in Appendix B).

## II. MODEL

The particle model we use is a hard triangular prism of height $h$, see Fig. 1(a). The orientation of the particle is defined by the Euler angles depicted in Fig. 1(b). The volume of the particle is $v = h\frac{\sqrt{3}l^2}{2}$, where $l$ is the length of the regular triangle's edges. We define the "width" of the triangular prisms via the circumference of the triangle $3l \equiv \pi w$, see Fig. 1(a). With that definition of width, the aspect ratio is $h/w$.

[a)]M. Marechal and S. Dussi contributed equally to this work.

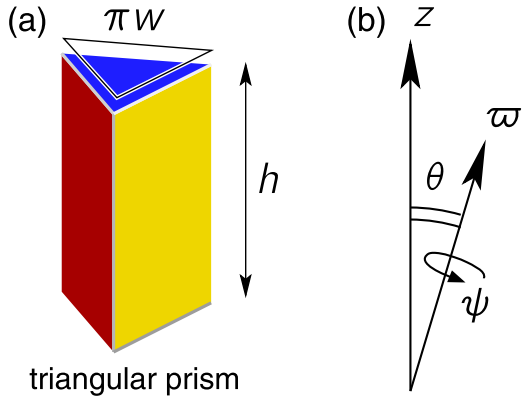


FIG. 1. (a) Triangular prism with an equilateral base. The height of the particle is $h$ whereas the width $w$ of the prism is defined as the circumference over $\pi$. (b) The Euler angles defining the orientation $\varpi$ of a particle where the $z$ axis is aligned with the nematic director. $\theta$ is the polar angle, $\phi$ is the azimuthal angle (not shown), and $\psi$ is the particle internal angle.

## III. DENSITY FUNCTIONAL THEORY: FUNDAMENTAL MEASURE THEORY

Density functional theory is specifically designed to handle inhomogeneous mixtures of anisotropic particles described by a density profile $\rho_s(\mathbf{r}, \varpi)$, which expresses the local density of particles of species $s$ orientation $\varpi$ at position $\mathbf{r}$, where $\varpi$ denotes the three Euler angles. The grand potential—the thermodynamic potential of the ensemble where the chemical potentials $\mu_s$, the volume $V$, and the temperature $T$ are held fixed—can be written as a sum over three parts

$$\Omega[\rho] = \mathcal{F}_{\mathrm{id}}[\rho] + \mathcal{F}_{\mathrm{exc}}[\rho] + \sum_s \int \mathrm{d}\varpi \int \mathrm{d}\mathbf{r}\rho_s(\mathbf{r}, \varpi)[V_s^{\mathrm{ext}}(\mathbf{r}, \varpi) - \mu_s], \tag{1}$$

where $V_s^{\mathrm{ext}}(\mathbf{r}, \varpi)$ is the external potential. The first term in the grand potential $\Omega$ is the ideal gas free energy,[10]

$$\mathcal{F}_{\mathrm{id}}[\rho] = k_{\mathrm{B}}T \sum_s \int\int \rho_s(\mathbf{r}, \varpi)\{\log[\rho_s(\mathbf{r}, \varpi)\mathcal{V}] - 1\}\,\mathrm{d}\varpi\,\mathrm{d}\mathbf{r}, \tag{2}$$

where $k_{\mathrm{B}}$ is Boltzmann's constant and $\mathcal{V}$ is the irrelevant thermal volume, which is the result of the integrals over the momenta conjugate to $\mathbf{r}$ and $\varpi$. We will use the (approximate) excess free energy $\mathcal{F}_{\mathrm{exc}}$ from fundamental measure theory (FMT).

In FMT[12,13,15,17,39] and variants,[19,20] hard-particle systems are connected to geometry by identifying a particle with species $s$ and coordinates $(\mathbf{r}, \varpi)$ with the set of points in its interior $\mathcal{B}_s(\mathbf{r}, \varpi)$. There are different versions of FMT, but all of them have an excess free energy of the form

$$\mathcal{F}_{\mathrm{exc}}[\rho] \equiv k_{\mathrm{B}}T \int \mathrm{d}\mathbf{r} \sum_{k=1}^{3} \Phi_k\left(\{n_\alpha[\rho](\mathbf{r})\}\right) \tag{3}$$

in three dimensions, where the $\Phi_k$ are functions of the (mixed) weighted densities $n_\alpha[\rho]$ that we will define shortly

$$\Phi(\{n_\alpha\}) = -n_0 \log(1 - n_3) + \frac{n_{12}}{1 - n_3} + C\frac{n_{222}}{(1 - n_3)^2}. \tag{4}$$

The differences between versions of FMT lie in the definitions of $n_{12}$ and $n_{222}$ and whether $C \neq 1$ is used to improve the third virial coefficient. The weighted densities $n_\alpha$ for $0 \leq \alpha \leq 3$ have units of (length)$^{\alpha-3}$ ($n_1$ and $n_2$ are introduced for later reference). These are related to the geometry of the particles, namely the topology, the integrated mean curvature, the surface area, and the volume of the particles for $\alpha = 0$, 1, 2, and 3, respectively. These are related to the geometry of the intersections of $n$ particles. A mixed[40] weighted density $n_A$ with multi-index $A = \alpha_1 \cdots \alpha_n$ has units of length to the power $\sum_{i=1}^{n}(\alpha_i - 3)$, such that each term in Eq. (4) has the units of density. Usually $n_{12}$ and $n_{222}$ are written in terms of a (tensor) product of single-index weighted densities of a tensorial nature.

The original version of FMT by Rosenfeld for hard spheres[17] has the disadvantage that it predicts the crystal of hard spheres to be unstable at all densities. To resolve this, an FMT for hard spheres was derived by demanding that the theory is exact in the so-called zero-dimensional limit, which is related to the crystal in the close-packed limit.[41] In this limit, the system is confined to such a great extent that only one particle with discrete positions and orientations fits in the volume of the system (in this case, the density profile is a sum of delta functions).[18,41] The resulting non-empirical version of FMT, which we will call 0D-FMT, can also be derived by approximating the virial series[42] and resumming the series to a closed form. This theory was deemed too unwieldy to use in FMT calculations for the hard sphere crystal, because $n_{222}$ could not be written in terms of single-index weighted densities (unlike previous versions); moreover, its prediction for the third virial coefficient of hard spheres is off. In the same publication[18] in which 0D-FMT was first derived, Tarazona and Rosenfeld solved both problems by approximating $n_{222}$ as an expression containing tensorial weighted densities of rank two and less and adjusting $C$ in Eq. (4) such that FMT yields the exact third virial coefficient for hard spheres; we will refer to Tarazona and Rosenfeld's version of FMT as TR-FMT. Later, additional improvements were proposed that lead to a very accurate DFT for hard spheres.[15,19–22]

After extending FMT to non-spherical particles, Rosenfeld realized that his original FMT would never predict a stable nematic phase.[39] A more careful extension of $n_{12}$ to non-spherical particles by Hansen-Goos and Mecke did lead to a DFT that can also describe the nematic phase,[12,13] while the functional can still be expressed in tensorial weighted densities of rank two and lower. However, an empirical rescaling was required for an accurate description of the isotropic–nematic transition. Afterwards,[30] it was found that the smectic phase was stable in a similarly extended TR-FMT but not in the more recent improved theories. Finally, it is possible to calculate $n_{12}$ exactly for non-spherical particles either by a direct calculation, which is computationally expensive, or an improved expansion in tensorial weighted densities.[31] We consider this theory as the proper extension of TR-FMT to non-spherical particles and refer to it simply as "TR-FMT." The predictions of TR-FMT for liquid crystals of hard spherocylinders are generally accurate, see Ref. 33 for an overview. Moreover, the semi-empirical constant introduced in Ref. 12 is removed from the theory. Nevertheless, the constant $C \neq 1$ in front of

the expression for $n_{222}$ is still somewhat empirical; furthermore, its value is obtained for hard spheres and thus might not be appropriate for non-spherical particles. For these reasons, we will also consider 0D-FMT, which has no adjustable constants ($C = 1$) and thus might be more robust under changes of the particle shape.

We will now give expressions for the weighted densities in the 0D-FMT functional and, subsequently, provide the differences between 0D-FMT and TR-FMT. First, the weighted density, $n_3$, is defined using an integral of the density profile over the particle volume

$$n_3[\rho](\mathbf{r}) = \sum_s \int \mathrm{d}\varpi \int_{\mathcal{B}_s(\mathbf{0},\varpi)} \mathrm{d}\mathbf{p}\, \rho_s(\mathbf{r}-\mathbf{p},\varpi). \tag{5}$$

Note that the integral over $\mathbf{p}$ runs over the interior of a particle centered around the origin; after a variable substitution $\mathbf{p} \to \mathbf{r}' = \mathbf{r} - \mathbf{p}$, Eq. (5) may also be interpreted as the sum over all species of the integral over all particle positions $\mathbf{r}'$ and orientations such that $\mathbf{r}$ lies inside $\mathcal{B}_s(\mathbf{r}',\varpi)$, the interior of a particle at $\mathbf{r}'$. The other weighted densities are defined using an integral over the particle surface in addition to an integral over the particle's orientations and a sum over the species (if applicable) or repeated integrals of this type, for which we define the shorthands

$$\int_{\{\partial\mathcal{B}_s(\mathbf{0},\varpi)\}} \mathrm{d}\mathfrak{R} \equiv \sum_s \int \mathrm{d}\varpi \int_{\partial\mathcal{B}_s(\mathbf{0},\varpi)} \mathrm{d}^2\mathbf{p}, \tag{6}$$

$$\int_{\{\partial\mathcal{B}_s(\mathbf{0},\varpi)\}^n} \mathrm{d}\mathfrak{R}^n \equiv \int_{\partial\mathcal{B}_{s_1}(\mathbf{0},\varpi_1)} \mathrm{d}\mathfrak{R}_1 \cdots \int_{\partial\mathcal{B}_{s_n}(\mathbf{0},\varpi_n)} \mathrm{d}\mathfrak{R}_n, \tag{7}$$

and finally, we define $\rho(\mathbf{r}-\mathfrak{R}_i) \equiv \rho_{s_i}(\mathbf{r}-\mathbf{p}_i,\varpi_i)$, where $\mathrm{d}^2\mathbf{p}$ denotes a surface area element at a point $\mathbf{p}$ on the boundary $\partial\mathcal{B}_s(\mathbf{0},\varpi)$ and $\mathfrak{R}_i = (\mathbf{p}_i, s_i, \varpi_i)$. With these shorthands, the (mixed) weighted density $n_A$, where $A$ has $n$ components, reads

$$n_A[\rho](\mathbf{r}) = \int_{\{\partial\mathcal{B}_s(\mathbf{0},\varpi)\}^n} \mathrm{d}\mathfrak{R}^n\, Q_A\left(\mathfrak{R}^n\right) \prod_{i=1}^{n} \rho(\mathbf{r}-\mathfrak{R}_i). \tag{8}$$

Similarly as for $n_3$, suitable variable substitutions allow the interpretation of Eq. (8) as the average of $Q_A$ over all particle positions, orientations, and species such that $\mathbf{r}$ simultaneously lies on the surfaces of all $n$ particles.

The function $Q_A\left(\mathfrak{R}^n\right)$ with $\mathfrak{R}_i = (\mathbf{p}_i, s_i, \varpi_i)$ for $i = 1,\ldots,n$ depends on the principal moments of curvature $\kappa_i^{\mathrm{I}}$ and $\kappa_i^{\mathrm{II}}$, the corresponding directions $\mathbf{v}_i^{\mathrm{I}}$ and $\mathbf{v}_i^{\mathrm{II}}$ and the normal vector $\mathbf{n}_i$ of the surface $\partial\mathcal{B}_{s_i}(\mathbf{0},\varpi_i)$ at the point $\mathbf{p}_i$ for all $i = 1,\ldots,n$. The explicit expressions for $Q_A$ read

$$Q_0(\mathfrak{R}_1) \equiv \frac{K_1}{4\pi}, \tag{9}$$

$$Q_{12}(\mathfrak{R}^2) \equiv \frac{\kappa_1^{\mathrm{II}}(\mathbf{v}_1^{\mathrm{I}}\cdot\mathbf{n}_2)^2 + \kappa_1^{\mathrm{I}}(\mathbf{v}_1^{\mathrm{II}}\cdot\mathbf{n}_2)^2}{4\pi(1+\mathbf{n}_1\cdot\mathbf{n}_2)}, \tag{10}$$

$$Q_{222}(\mathfrak{R}^3) \equiv |(\mathbf{n}_1\times\mathbf{n}_2)\cdot\mathbf{n}_3| \frac{2\pi - 3\,\alpha(\mathbf{n}_1,\mathbf{n}_2,\mathbf{n}_3)}{24\pi}, \tag{11}$$

where $K_i = \kappa_i^{\mathrm{I}}\kappa_i^{\mathrm{II}}$ is the Gaussian curvature and $\alpha(\mathbf{n}_1,\mathbf{n}_2,\mathbf{n}_3)$ is the angle between the two cross products,[43] $\mathbf{n}_1\times\mathbf{n}_2$ and $\mathbf{n}_2\times\mathbf{n}_3$.

The only quantities that are different in TR-FMT compared to 0D-FMT are the value for the adjustable constant $C = 9$ and the form for $Q_{222}$,[18]

$$Q_{222}(\mathfrak{R}^3) \simeq Q_{222}^{\mathrm{TR}}(\mathfrak{R}^3) \equiv \frac{1}{48\pi}[\mathbf{n}_1\cdot(\mathbf{n}_2\times\mathbf{n}_3)]^2, \tag{12}$$

which reduces to $Q_{222}$ in the limit that the normal vectors become parallel.[42]

The high dimensionality of the integrals over $\mathfrak{R}^n$ in the definition of the mixed weighted densities $n_{12}$ for TR-FMT and 0D-FMT and $n_{222}$ for 0D-FMT makes it difficult to evaluate them (practically impossible in case of $n_{222}$ for the smectic phase). Therefore, we follow Wertheim[44] in expanding the $n_A$ in terms of spherical harmonics. While this expansion is new in the case of $n_{222}$ and has never been applied to FMT, the (analytic) calculation of the coefficients is somewhat involved, so we present it in Appendix A. The result has the typical form for FMT

$$n_{12}(\mathbf{r}) = \sum_{\vec{l}} n_1^{(\vec{l})}(\mathbf{r}) n_2^{(\vec{l})}(\mathbf{r}), \tag{13}$$

$$n_{222}(\mathbf{r}) = \sum_{\vec{l}_1,\vec{l}_2,\vec{l}_3} C_{222}^{(\vec{l}_1,\vec{l}_2,\vec{l}_3)} n_2^{(\vec{l}_1)}(\mathbf{r}) n_2^{(\vec{l}_2)}(\mathbf{r}) n_2^{(\vec{l}_3)}(\mathbf{r}), \tag{14}$$

where $\vec{l}_i = (l_i, m_i)$ with the degree $l_i$ and order $m_i$ of a spherical harmonic and the weighted densities $n_\alpha^{(\vec{l})}$ for $\alpha = 1, 2$ are defined by

$$n_\alpha^{(\vec{l})}(\mathbf{r}) = \sum_s \int \mathrm{d}\varpi \left[\int \mathrm{d}\mathbf{r}'\, w_\alpha^{(\vec{l})}(\mathbf{r}-\mathbf{r}', s, \varpi)\rho_s(\varpi,\mathbf{r}')\right], \tag{15}$$

where the expression in square brackets is a convolution of a weight function and the density profile that can be efficiently calculated using fast Fourier transforms (see Appendix B). Here, $w_\alpha^{(\vec{l})}(\mathbf{r}, s, \varpi)$ are the weight functions (proportional to a one-dimensional delta-function) defined in Eqs. (A40)–(A42). The method for calculating the weighted densities for polyhedra is given in Appendix B and Ref. 29.

For the minimization of the grand potential with respect to the density profile, we employ either a variational approach, where the density profile is parametrized as described in Ref. 30, or we perform a full minimization using Picard iteration on a grid.[48] In either case, the density profile is calculated on a two-dimensional grid consisting of equidistant points in the $z$-direction and, in the $\theta$-direction, either a fine equidistant grid or the points from a modified Gauss-Legendre quadrature. For the modified Gauss-Legendre quadrature, we first performed a variable transformation $\theta \to x = \sinh(\lambda\cos\theta)$ with $\lambda$ chosen such that $\cosh(\lambda\theta)$ approximates the expected $\theta$-dependence of the density profile (see Ref. 49 for the reasoning behind performing such a variable transformation). We also performed full minimizations on three-dimensional $(z,\theta,\psi)$ grids, but we never found significant $\psi$-dependence of the density profile.

## IV. SECOND-VIRIAL DFT: ISOTROPIC-NEMATIC TRANSITION

To describe the isotropic-nematic transition, we also use a second-virial (Onsager-like[50]) density functional theory that

we compare against results from FMT and simulations. In this case, we do not fully consider the biaxial nature of the particle shape in the description of the nematic order. In particular, we assume that the single-particle density of the homogeneous bulk nematic phase can be written as $\rho(\mathbf{r}, \varpi) = \bar{\rho}\,\varphi(\theta)$, with $\bar{\rho} = N/V = \eta/v$ the number density, $V$ the volume of the system, $v$ the particle volume, and $\eta$ the packing fraction of the system. The orientation distribution function $\varphi$ depends only on the polar angle $\theta$ (see Fig. 1(b)) and the free energy of the system is

$$\frac{\beta\mathcal{F}[\varphi]}{V} = \bar{\rho}(\log \mathcal{V}\bar{\rho} - 1) + 4\pi^2\bar{\rho}\int d\cos\theta\,\varphi(\theta)\log\varphi(\theta) + G(\eta)\frac{\bar{\rho}^2}{2}\int d\cos\theta\, d\cos\theta' E(\theta,\theta')\varphi(\theta)\varphi(\theta') \tag{16}$$

with $\beta = 1/k_B T$, $\mathcal{V}$ the irrelevant thermal volume, and $G(\eta) = (1-\frac{3}{4}\eta)/(1-\eta)^2$ the Parsons-Lee correction factor.[51,52] The excluded volume between two particles with orientation $\varpi$ and $\varpi'$, respectively, and separated by a distance $\mathbf{r}$ is given by

$$E(\theta,\theta') = -\int d\phi\, d\phi'\, d\psi\, d\psi' d\mathbf{r} f(\mathbf{r},\varpi,\varpi') \tag{17}$$

with $f(\mathbf{r},\varpi,\varpi') = \exp(-\beta U(\mathbf{r},\varpi,\varpi')) - 1$ the Mayer function, $U(\mathbf{r},\varpi,\varpi')$ the (hard-core) pair potential, and $\phi$ and $\psi$ the azimuthal and internal angle (see Fig. 1(b)). In practice, the excluded volume is computed by performing a Monte Carlo (MC) integration over many randomly generated pairs of particles, by checking if they overlap using an algorithm based on the Robust and Accurate Polygon Interface Detection (RAPID) library.[53] This procedure has been already used, for example, to describe the chiral nematic order in similar systems composed of twisted triangular prisms.[54] In summary, the excluded volume used as input for the (Parsons-Lee) Onsager theory is an average over the particle internal angle. The free-energy functional is minimized subject to the normalization condition $\int d\varpi\varphi(\theta) = 1$. The resulting non-linear equation for the orientation distribution function reads

$$\varphi(\theta) = \frac{1}{Z}\exp\left(-\bar{\rho}G(\eta)\int d\cos\theta'\frac{E(\theta,\theta')}{4\pi^2}\varphi(\theta')\right), \tag{18}$$

where $Z$ is a normalization constant. Eq. (18) is solved self-consistently at fixed density $\bar{\rho}$ by using a discrete grid for the polar angle $\theta$ (see, e.g., Ref. 55). The resulting equilibrium orientation distribution function $\varphi_{eq}(\theta)$ is used to calculate the relevant thermodynamic and structural quantities, such as the nematic order parameter

$$S = \int d\theta\left[\frac{3}{2}\cos^2(\theta) - \frac{1}{2}\right]\varphi_{eq}(\theta). \tag{19}$$

## V. COMPUTER SIMULATIONS

To study the phase behavior of hard elongated triangular prisms, we employ standard Monte Carlo (MC) simulations either in the *NPT* or in the *NVT* ensemble.[56] We use $N = 2000$ particles with different aspect ratios $h/w \in [3.0, 6.0]$ and several millions of MC steps are performed for typical runs. For *NVT*-MC simulations, each MC step consists on average of $N/2$ attempts of translating a random particle and $N/2$ attempts of rotating a random particle. For *NPT*-MC simulations, an additional attempt to either scale isotropically the volume or to change only one edge of the cuboidal simulation box is tried at each MC step. The particles interact via a hard-core potential only. To detect overlaps between particles, we use an algorithm, based on the RAPID library,[53] that consists in detecting the intersections between the (rectangular or triangular) faces of the polyhedral particles.

To quantify the orientational and positional order in the system, we use standard order parameters. First, we construct the nematic order parameter tensor

$$\mathcal{Q}_{\alpha\beta} = \frac{1}{N}\sum_{i=1}^{N}\left[\frac{3}{2}\hat{\mathbf{u}}_{i\alpha}\hat{\mathbf{u}}_{i\beta} - \frac{\delta_{\alpha\beta}}{2}\right], \tag{20}$$

where $\alpha, \beta = x, y, z$ component, $\hat{\mathbf{u}}$ denotes the particle long axis, $N$ is the number of particles, and $\delta_{\alpha\beta}$ the Kronecker delta. After diagonalizing $\mathcal{Q}$, we identify the (scalar) order parameter $S$ as the maximum eigenvalue. The associated eigenvector corresponds to the nematic director $\hat{\mathbf{n}}$. Similar nematic order parameter tensors can be calculated considering the short and the medium particle axes, thereby probing oblate (or discotic-like) order in the system. Furthermore, it is also possible to quantify the degree of (macroscopic) biaxial alignment of a nematic phase by defining an additional order parameter, as, for example, used in Ref. 57. However, for the particle shapes studied in the present work, we observe only the formation of uniaxial prolate (or calamitic) nematic phases. The results on similar particle shapes forming prolate and biaxial nematic phases have been anticipated in Ref. 54 and will be reported in detail elsewhere.

To identify the phase transition to a smectic phase, we monitor the onset of positional order along the nematic director $\hat{\mathbf{n}}$ and we calculate the smectic order parameter defined as

$$\tau = \max_{l\in\mathbb{R}}\left|\sum_{j=1}^{N}\exp\left(\frac{2\pi}{l}i\mathbf{r}_j\cdot\hat{\mathbf{n}}\right)\right|, \tag{21}$$

where $\mathbf{r}_j$ denotes the position of particle $j$.

## VI. RESULTS

We first report the liquid crystal behavior of hard triangular prisms as obtained using MC simulations that will be compared below with the theoretical predictions. The equation of state is obtained after long equilibration runs in the *NPT* ensemble, typically expanding from close-packed configurations, and averaging the density over equilibrated configurations generated in the last $\sim 10^6$ MC steps. In Fig. 2(a), we plot the reduced pressure $\beta P w^3$, with $\beta = 1/k_B T$, $T$ the temperature, and $k_B$ the Boltzmann constant, as a function of the packing fraction $\eta$ for some of the systems studied. We find an isotropic (I) phase at low densities and a crystal (X) phase at high densities for all the aspect ratios $h/w \in [3.0, 6.0]$. For $h/w = 3$, we observe a clear jump in the density that corresponds to a first-order transition from I to a smectic (Sm) phase. In the case of longer particles, a

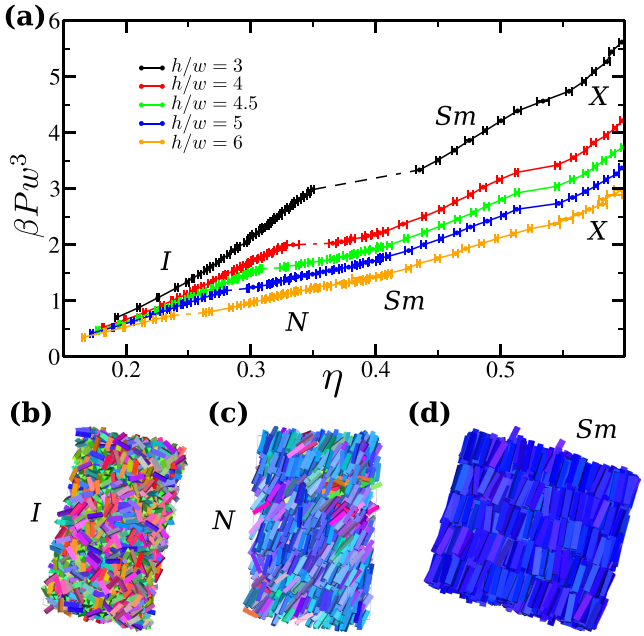


FIG. 2. (a) Equations of state (reduced pressure $\beta P w^3$ versus packing fraction $\eta$) obtained by MC-*NPT* simulations for triangular prisms with different aspect ratio $h/w$ along with representative snapshots of (b) an isotropic (I) phase, (c) a nematic (N) phase, and (d) a smectic (Sm) phase. Particles are colored according to the orientation of their long axis. At high densities, the triangular prisms form a crystal phase (X).

nematic (N) phase is also observed, and the jumps in densities associated with the I-N and N-Sm transitions are barely visible.

Both in the nematic phase and in the smectic phase, only the long particle axis exhibits long-range orientational order, as evident from visual inspection of typical configurations, shown in Figs. 2(c) and 2(d), and further confirmed by the order parameter analysis. The liquid crystal behavior is therefore qualitatively similar to that of spherocylinders (uniaxial rod-like particles) with comparable aspect ratio.[58] The phase transitions can be determined by identifying the jumps of the nematic order parameter $S$ and the smectic order parameter $\tau$ as a function of the packing fraction $\eta$, as shown in Fig. 3. For $h/w = 3$, we can clearly identify an I-Sm transition since both $S$ and $\tau$ simultaneously jump in correspondence to the large density jump. A direct transition from I to Sm can also be observed for $h/w = 4$, despite the smectic order parameter $\tau$ displaying a less abrupt jump. For larger aspect ratios, a N phase appears in between the I and the Sm phase. A weakly first-order N-Sm transition is observed for triangular prisms with $h/w = 4.1$ and $h/w = 4.3$, since $\tau$ displays a jump at larger $\eta$ than $S$, and this is further confirmed by the visual inspection of the configurations. Longer triangular prisms exhibit more pronounced jumps of the order parameters. We can conclude that triangular prisms with $h/w \gtrsim 4$ self-assemble into a N phase. For larger $h/w$, the I-N transition clearly shifts towards smaller $\eta$ whereas the location of the N-Sm is less sensitive to $h/w$.

We now compare the equation of state as obtained by computer simulations with that calculated by using the two versions of FMT.

The equation of state for the homogeneous fluid can be obtained from a density functional theory by inserting a constant density profile $\rho(\mathbf{r}, \varpi) = \eta/v$. In this case, all weighted densities are also constant and only the scalar weighted densities (i.e., those with $l = 0$ and $m = 0$) are nonzero

$$n_\alpha^{(l,m)}(\mathbf{r}) = \delta_{l,0}\delta_{m,0}\,\xi_\alpha \eta/v, \tag{22}$$

where the $\xi_\alpha$ are the so-called fundamental measures of the particle: $\xi_0$ is a topological invariant, which is equal to one for all simply connected particles; $\xi_1 = \frac{3l}{8} + \frac{h}{4}$ is the mean-half width (proportional to the integrated mean curvature); $\xi_2 = \frac{\sqrt{3}\,l^2}{2} + 3\,h\,l$ is the area, and $\xi_3 = v = \frac{\sqrt{3}\,l^2}{4}$ is the volume of the triangular prism. Furthermore,

$$C_{222}^{(0,0,0,0,0,0)} = \frac{\pi}{384} \quad \text{and} \quad C_{\mathrm{TR}}^{(0,0,0,0,0,0)} = \frac{1}{216\pi}, \tag{23}$$

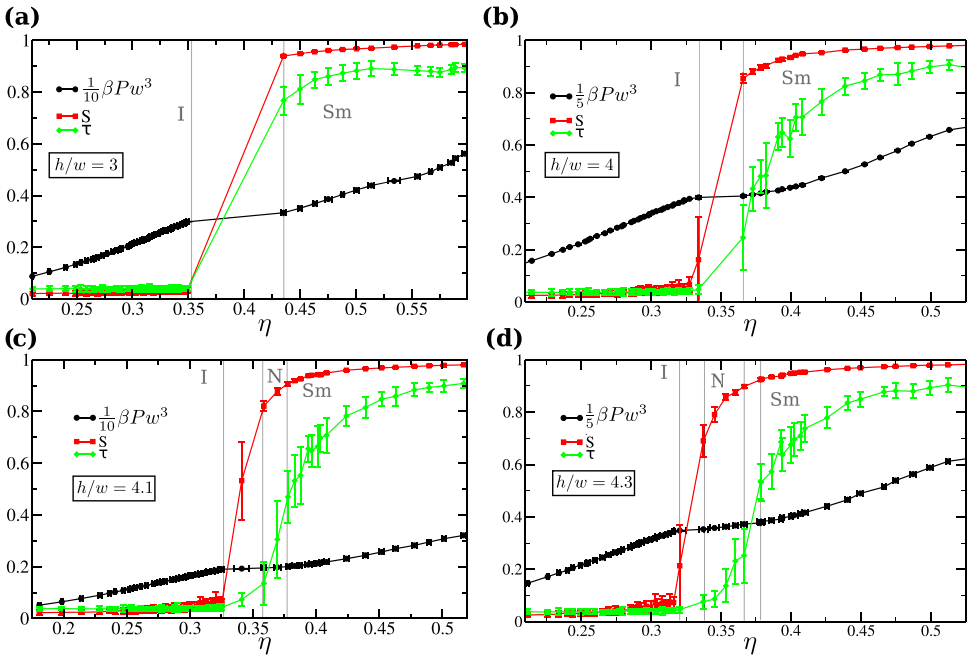


FIG. 3. Reduced pressure $\beta P w^3$, nematic order parameter $S$, and smectic order parameter $\tau$ versus packing fraction $\eta$ for triangular prisms with (a) $h/w = 3$, (b) $h/w = 4$, (c) $h/w = 4.1$, and (d) $h/w = 4.3$. Vertical lines are guides-to-the-eye to locate the jumps in the order parameters and therefore estimate the phase transitions.

see Subsection 2 of Appendix A. Therefore, the pressure as calculated from $-(\partial F/\partial V)_N$ with $F = \mathcal{F}[\rho] = \mathcal{F}_{\rm id}[\rho] + \mathcal{F}_{\rm exc}[\rho]$ from FMT reads

$$\frac{\beta P}{\rho} = \frac{1 + (c_1 - 2)\,\eta + (2\,c_2 - c_1 + 1)\,\eta^2}{(1-\eta)^3}, \qquad (24)$$

where $c_1 = \frac{\xi_1 \xi_2}{\xi_3}$ and $c_2 = C_{222}^{(0,0,0,0,0,0)} \frac{\xi_2^3}{\xi_3^2} = \frac{\pi}{384} \frac{\xi_2^3}{\xi_3^2}$ for 0D-FMT and $c_2 = 9 C_{TR}^{(0,0,0,0,0,0)} \frac{\xi_2^3}{\xi_3^2} = \frac{1}{24\pi} \frac{\xi_2^3}{\xi_3^2}$ for TR-FMT. For TR-FMT, Eq. (24) is the usual scaled particle equation of state, which reduces to the Percus-Yevick equation of state (from the compressibility route) for spheres. The EOS from 0D-FMT is not a very good one for the homogeneous fluid of spheres,[18] but it is interesting to see how it performs for triangular prisms. For the nematic phase and the smectic phase, we calculated the pressure within TR-FMT and 0D-FMT by numerically calculating the derivative $-(\partial F/\partial V)_N$, where the free energy $F$ was obtained by minimizing $\mathcal{F}[\rho]$ with respect to $\rho$ at a constant average density using a variational approach.[30]

The resulting equation of state is shown in Fig. 4 and compared to the simulation results (we have not considered the crystal in FMT) for triangular prisms with $h/w = 3$ and $h/w = 6$. It can be seen that the equation of state from TR-FMT is more accurate than that of 0D-FMT especially for the longer particles. Surprisingly, TR-FMT is more accurate for longer prisms than for shorter ones. We would not necessarily expect TR-FMT to perform well for long particles since the value for $C$ in Eq. (4) is chosen such that it gives a good EOS for spheres. The less empirical theory, 0D-FMT, seems to have a consistent deviation from the simulation result; in particular, it always overestimates the pressure for the smectic phase. In the remainder of this paper, we will employ TR-FMT as it generally performs better than 0D-FMT concerning both the accuracy and the computational efficiency.

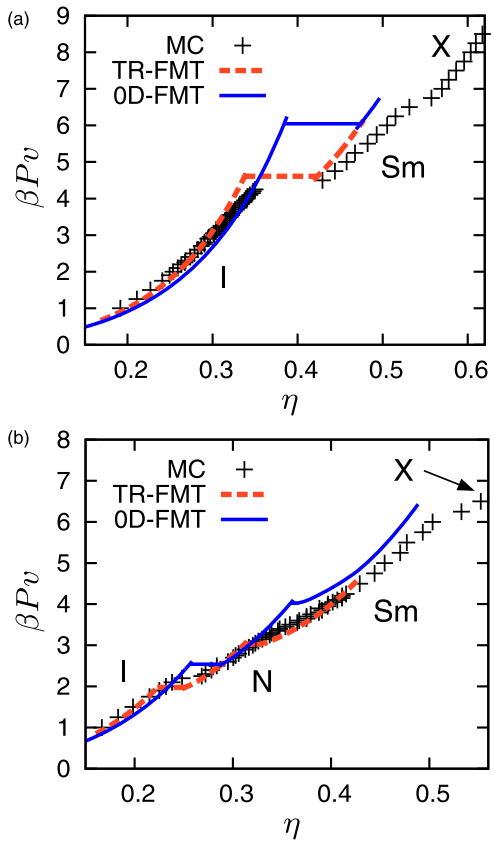


FIG. 4. Comparison between the equations of states, pressure $\boldsymbol{P}$ versus packing fraction $\eta$, from simulations (MC) and the functionals 0D-FMT and TR-FMT for hard triangular prisms with aspect ratios (a) $h/w = 3$ and (b) $h/w = 6$.

In order to obtain more insight into the performance of (TR-)FMT, we will now compare the results for the nematic order parameter with simulations and also with results obtained by using the second-virial Onsager-Parsons-Lee theory (described in Sec. IV). In Fig. 5, we plot the dependence of the nematic order parameter $S$ on the packing fraction $\eta$ as

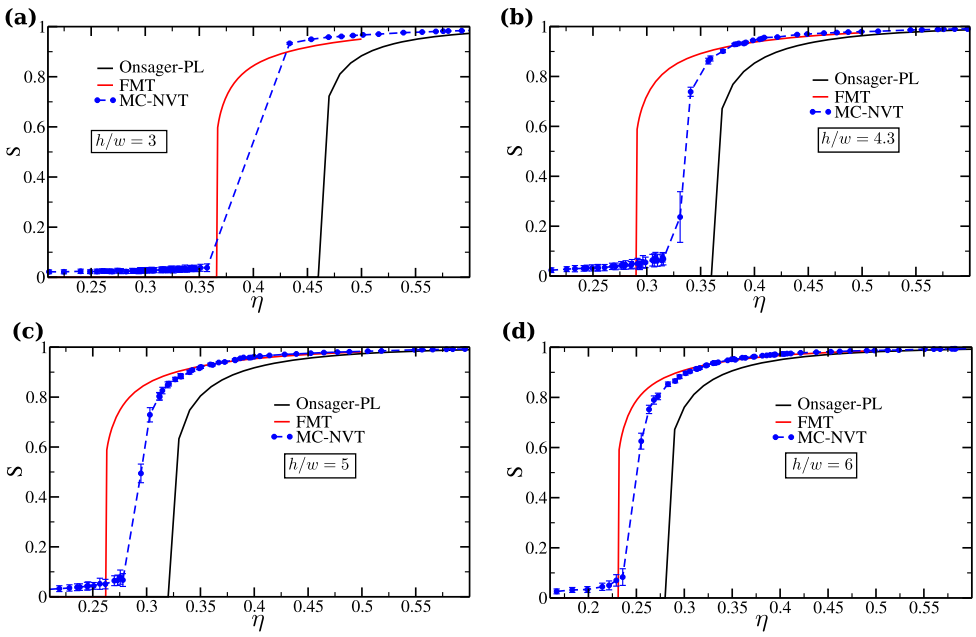


FIG. 5. Nematic order parameter $S$ versus packing fraction $\eta$ as obtained by MC-$NVT$ simulations, by Onsager theory with Parsons-Lee (PL) correction, and by TR-FMT, for triangular prisms with (a) $h/w = 3$, (b) $h/w = 4.3$, (c) $h/w = 5$, and (d) $h/w = 6$.

obtained by the three different methods, for triangular prisms with different $h/w$. We observe that Onsager-PL theory largely overestimates the packing fraction at which the I-N transition occurs, confirming the known drawback of such a theory. On the other hand, FMT predictions for the jump of $S$ match well with the simulation results for triangular prisms with $h/w = 3$, for which only the I-Sm transition occurs. On the other hand, as soon as the N phase becomes stable, e.g., for $h/w = 4.3$, the FMT underestimates the packing fraction associated with the jump of $S$. However, upon increasing aspect ratio $h/w$, the discrepancy diminishes and already for $h/w = 6$ a good agreement for the I-N transition is obtained.

The nematic order parameter is only the second moment for the distribution $\varphi(\cos\theta)$, where $\theta$ is the angle between the director of the nematic phase and the long axis of the particle. In Fig. 6, we compare the full distribution from FMT to the simulated profile. Clearly, the prediction for the distribution from FMT is quite good, except for the larger angles that have a very low $\varphi(\cos\theta)$ and thus hardly contribute to ensemble averages. We show that the deviation is mostly due to an incorrect prediction of the order parameter by performing an FMT calculation at a lower density where the nematic order parameter $S$ equals that of the computer simulations. The profile $\varphi(\theta)$ from this calculation (the short-dashed line in Fig. 6) agrees almost perfectly with the simulated $\varphi(\theta)$. We also show the orientational distribution from Ref. 30 as the long-dashed line in Fig. 6. The deviation between the parametrized orientational distribution and the exact minimum is small, clearly much smaller than the deviation between DFT and the simulation results. Therefore, we feel a full minimization on a grid is not warranted and we will use the parametrized variational approach in the remainder, also for the smectic phase.

Finally, we superimpose the simulations results in Fig. 7 together with the phase diagram obtained by the FMT, where we employ the aspect ratio $h/w$—packing fraction $\eta$ representation. For the simulation results, we estimate the phase

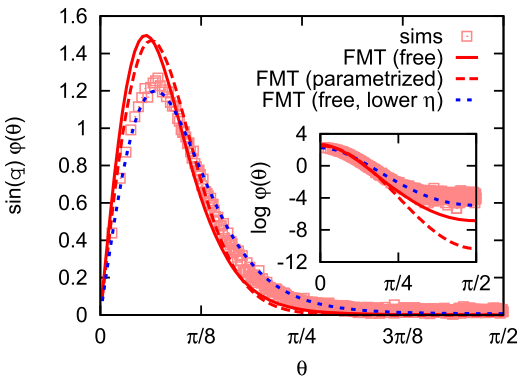


FIG. 6. The orientational distribution, $\varphi(\theta)$ [see Fig. 1(b) for the definition of $\theta$]: $\sin\theta\,\varphi(\theta)$ and $\log\varphi(\theta)$ (inset) as a function of $\theta$ for an aspect ratio $h/w = 5$. Simulation results are shown for the nematic phase for $\eta = 0.311\,666$ (red squares) and these are compared to TR-FMT results for the same density (solid and long-dashed red lines) and a different density $\eta = 0.286$ (short-dashed blue line) at which the nematic order parameter $S$ is approximately equal to that of the simulation at $\eta = 0.311\,666$. The solid and short-dashed lines correspond to a free minimization on a grid and the long-dashed line corresponds to a parametrized minimization.[30]

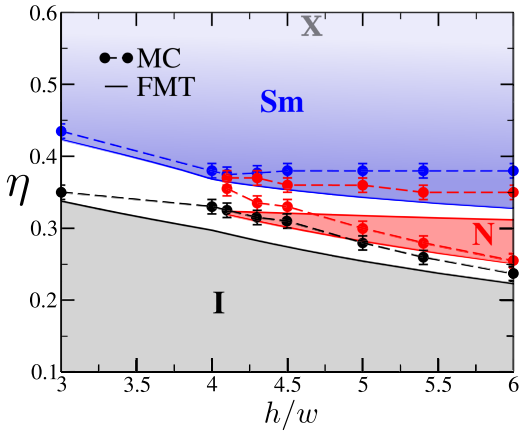


FIG. 7. Phase diagram obtained by TR-FMT (solid lines) compared with simulation results (symbols) in the aspect ratio $h/w$–packing fraction $\eta$ representation. Isotropic (I) stability region is colored gray, nematic (N) red, smectic (Sm) blue, and coexistence regions white. The boundaries for the crystal phase (X) are not calculated explicitly.

boundaries based on the order parameters and by considering the upper and lower packing fraction at which a given phase is observed. We estimate the degree of uncertainty in the identification of the phase boundaries and plot the coexisting densities in $\eta$ with the estimated error bar of 0.01 in Fig. 7.

We confirm once more that the overall qualitative liquid-crystal behavior of triangular prisms is well captured by FMT that also predicts a stable nematic phase for triangular prisms with $h/w > 4.0$. No biaxial order was observed in simulations or predicted by FMT, neither for the nematic nor for the smectic phase. As was already found for spherocylinders,[30,31] TR-FMT predicts the smectic phase to be more stable than it actually is, especially for longer particles. The less-empirical theory, 0D-FMT, more accurately predicts the area of stability of the smectic phase, as can be seen from the tie-lines in Fig. 4. However, this is most likely a cancellation of errors, as the quality of the EOS from 0D-FMT is considerably worse than the one from TR-FMT.

Interestingly, the smectic phase is stable at a considerably lower packing fraction for prisms than for spherocylinders[31,58] in both FMT and simulations. Despite the two particle models have different shapes, we can try to compare their phase behavior assuming that triangular prisms with $h/w = h^*$ behave similar to spherocylinders with $(L+D)/D = h^*$, with $L$ the cylinder length and $D$ the particle diameter (which coincides with the diameter of the two hemispherical caps). If this analogy holds, we observe that a nematic phase is stabilized for triangular prisms with $h^* \gtrsim 4$ and for spherocylinders with $h^* > 4.7$. Furthermore, in this range of $h^*$, the smectic phase can be stabilized at lower packing fraction $\eta$ in the case of triangular prisms ($\eta \lesssim 0.4$) than for spherocylinders ($\eta \gtrsim 0.45$).

## VII. SUMMARY AND DISCUSSION

We have considered the liquid crystal phases of triangular prisms using both simulations and density functional theory (DFT), with the following goals: (1) we investigated the accuracy of a recently (re)derived theory, 0D-FMT[42] compared to

the more established theory TR-FMT[18] and (2) we were interested in the effect of the shape of the particles beyond their overall rod-like shape. Regarding the first point, we showed that TR-FMT generally performs better than 0D-FMT irrespective of particle aspect ratio. We should note that TR-FMT has undergone a minor empirical modification (in the $C$-factor in Eq. (4)). It is possible that a similar modification to 0D-FMT leads to a similar improvement, although our preliminary attempts have been unsuccessful.

Regarding the effect of the particle shape, we found that the smectic phase is stabilized relative to the nematic phase compared to the commonly studied spherocylinders.[58] In other words, both the packing fraction of the nematic phase $\eta_{\mathrm{N}}$ and that of the smectic phase $\eta_{\mathrm{Sm}}$ at coexistence between the two phases are lower for triangular prisms than for spherocylinders. These results hold regardless whether simulations or FMT calculations are used to obtain the phase diagram. We can make this observation without a well-motivated shape characteristic because $\eta_{\mathrm{N}}$ and $\eta_{\mathrm{Sm}}$ depend only weakly on the particle aspect ratio. For square prisms (or cuboids),[37,38] $\eta_{\mathrm{N}}$ and $\eta_{\mathrm{Sm}}$ also decrease compared to the values for spherocylinders. However, $\eta_{\mathrm{N}}$ and $\eta_{\mathrm{Sm}}$ depend strongly on the aspect ratio for square prisms and the decrease of the $\eta_N$ and $\eta_{\mathrm{Sm}}$ is not as large as what we observed for triangular prisms.[37,38] Clearly, the shape of the prism base matters.

Future work could attempt to distinguish further between the effects of the shape of the base and the flat top and bottom faces compared to the spherical caps of spherocylinders, for example, by considering cylinders. Since TR-FMT correctly predicted the decrease of $\eta_{\mathrm{N}}$ and $\eta_{\mathrm{Sm}}$, this theory can be used to perform such an investigation. Furthermore, we will investigate, by varying the triangular cross section of the particle, when oblate and biaxial nematic phases become stable and if the theoretical framework is able to correctly capture the features of the different order.

Another possible avenue of research as far as the theory is concerned is an empirical modification of 0D-FMT. However, 0D-FMT has two desirable properties that other versions of FMT do not: First, the dimensional reduction through confinement is consistent with a direct derivation for the lower dimensional system. Consequently, the exact description of quasi-0D and 1D systems (for which the direct derivation leads to the exact free energy) is obtained automatically. For other versions of FMT, correct behavior under quasi-0D and 1D confinement has to be imposed during the derivation. Second, the excess free energy is correctly invariant under anisotropic scaling of the entire system (including the shape of the particles) as used in Ref. 58; in fact, invariance under any linear transformation should be obeyed and is obeyed by 0D-FMT. A further exact relation that is obeyed by most versions of FMT[15,17,18] is the scaled particle relation,[17,42] which relates the mechanical work required to insert a macroscopically large particle in the system to the chemical potential of such a very large particle. This property can be (partially[20]) violated when the functional undergoes empirical modifications[19] to improve the equation of state. Which of these properties is more important for studies of liquid crystals and phase behavior of hard particles in general is another possible topic for further research.

## ACKNOWLEDGMENTS

S.D. and M.D. acknowledge financial support from a NWO-ECHO grant and M.M. and from the German research foundation (DFG) through the research unit "Geometry of spatially random systems." M.M. thanks Klaus Mecke and René Wittmann for fruitful discussions.

## APPENDIX A: EXPANSION OF THE $Q_A$ FUNCTIONS

We will calculate $Q_A$ for $A = 12$ and $A = 222$ using an expansion of the form[45]

$$Q_A(\mathfrak{R}^n) = \sum_{\vec{l}_1,\ldots,\vec{l}_n} C_A^{(\vec{l}_1,\ldots,\vec{l}_n)} \prod_{i=1}^{n} q_{\alpha_i}^{(\vec{l}_i)}(\mathfrak{R}_i), \tag{A1}$$

where the functions $q_{\alpha_i}^{(\vec{l})}$ and the constants $C_{\alpha}^{(\vec{l}_1,\ldots,\vec{l}_n)}$ will be determined in Subsection 1 of Appendix A for $Q_{12}$ and Subsection 2 of Appendix A for $Q_{222}$. The $Q_{222}^{\mathrm{TR}}$ function from TR-FMT has the large advantage that it can be expressed (exactly) as a finite sum of the form (A1) with coefficients $C_{\mathrm{TR}}^{(l_1,m_1,l_2,m_2,l_2,m_3)}$, which are calculated in Subsection 3 of Appendix A.

Like all numerical methods, the expansions of $Q_{12}$ and $Q_{222}$ (in 0D-FMT) have errors due to the truncation of the infinite sum at a finite order $l_{\max}$. The number of terms in the expansions of $Q_{12}$ and $Q_{222}$ scale with $l_{\max}^2$ and $l_{\max}^5$ for the general case in 0D-FMT. As we only consider phases with at least two continuous translational symmetries and one rotational symmetry, the $n_{\alpha}^{(l,m)}$ with $m \neq 0$ vanish. Therefore, the number of terms in $Q_{12}$ scales with $l_{\max}$ and the number of terms in $Q_{222}$ scales with $l_{\max}^3$. We used $l_{\max} = 64$ in this work, which leads to a numerical error that is negligible in comparison to the difference between the simulations and the theory. It should be noted that the system we have chosen to study presents a worse case scenario as the long prisms are strongly aligned in the smectic phase. This results in a strong alignment of the normals to the top and bottom surfaces with the director and nearly $\delta$-function-like contributions in the averages over $\mathbf{n}_2$ in $n_{12}$ and $\mathbf{n}_i$ in $n_{222}$. As the accurate resolution of those peaks requires a large number of spherical harmonics, we expect that this is the reason why we needed such high truncation orders in $l$ and that much less effort is required to handle most other phases and particles.[46]

### 1. Second term: $Q_{12}$

The expansion proposed for $Q_{12}$ by Wertheim[44] (outside of the context of density functional theory) uses the observation that $Q_{12}(\mathfrak{R}_1, \mathfrak{R}_2) = Q_{12}(\mathfrak{R}_1, \mathbf{n}_2)$ only depends on $\mathfrak{R}_2$ through the normal vector $\mathbf{n}_2$, such that we can expand $Q_{12}$ in the orthonormal spherical harmonics $Y_l^m(\mathbf{n}_2)$, which amounts to the expansion of the form (A1) with the definitions

$$q_1^{(l,m)}(\mathfrak{R}) = \int_{S^2} \mathrm{d}\mathbf{n}\, Q_{12}(\mathfrak{R}, \mathbf{n}) Y_l^m(\mathbf{n}) N_l^0, \tag{A2}$$

$$q_2^{(l,m)}(\mathfrak{R}) = Y_l^{m*}(\mathbf{n}(\mathfrak{R}))/N_l^0, \tag{A3}$$

and $C_{12}^{(l_1,m_1,l_2,m_2)} = \delta_{l_1,l_2}\delta_{m_1,m_2}$ (the latter is a consequence of symmetry under a rotation of the whole system including the

density profile and the external potential). We divided $q_2^{(l,m)}$ by $N_l^0 = \sqrt{(2l+1)/(4\pi)}$ to simplify the expression for $q_1^{(l,m)}$ with $l = 0, 1$ and to recover the usual scalar FMT weighted densities $n_\alpha$ for $\alpha = 1, 2$: $n_\alpha^{(0,0)} = n_\alpha$.

An analytical form for $q_1^{(l,m)}$ has been obtained by Wertheim (who uses a different notation)[44] and we will give his calculation in our notation now.

The conceptually difficult step in the calculations of both $q_1^{(l,m)}$ and $C_{222}^{(\vec{l}_1,\vec{l}_2,\vec{l}_3)}$ involves parametrizing the normal vectors in the (innermost) integral using spherical coordinates with respect to a properly chosen basis $\{\mathbf{b}_i\}$ and subsequently using the property of the spherical harmonics

$$Y_l^{\mathsf{T}}(\theta', \phi') = Y_l^{\mathsf{T}}(\theta, \phi)\mathcal{D}^l(\mathcal{R}), \tag{A4}$$

where $\mathcal{R}$ is the rotation from the lab frame, $\{\mathbf{e}_i\}$, to the basis $\{\hat{b}_i\}$, i.e., $\hat{b}_i = \mathcal{R}\mathbf{e}_i$; the angles $\phi$, $\theta$, $\phi'$, and $\theta'$ are defined by $(\cos\phi\mathbf{e}_1 + \sin\phi\mathbf{e}_2)\sin\theta + \cos\theta\mathbf{e}_3 = (\cos\phi'\hat{b}_1 + \sin\phi'\hat{b}_2)\sin\theta' + \cos\theta'\hat{b}_3$; $Y_l$ is a $(2l+1)$-dimensional (column) vector with components $Y_l^m$ for $-l \le m \le l$; and $\mathcal{D}^l$ is the Wigner $D$ matrix of order $l$ with components $\mathcal{D}^l_{mn}$ for $-l \le m, n \le l$.

For $q_1^{(l,m)}$, we write the normal vector $\mathbf{n}_2$ as

$$(\cos\phi_{12}\,\mathbf{v}_1^{\mathrm{I}} + \sin\phi_{12}\,\mathbf{v}_1^{\mathrm{II}})\sin\theta_{12} + \cos\theta_{12}\,\mathbf{n}_1, \tag{A5}$$

that is, we use the basis $\{\mathbf{b}_i\} = \{\mathbf{v}_1^{\mathrm{I}}, \mathbf{v}_1^{\mathrm{II}}, \mathbf{n}_1\}$. We obtain (see also Ref. 44)

$$Q_{12}(\mathfrak{R}^2) = \frac{(1-\cos\theta_{12})}{4\pi}[H_1 - \Delta\kappa_1\cos(2\phi_{12})]. \tag{A6}$$

We will expand this in spherical harmonics, which can be written as

$$Y_l^m(\theta,\phi) = \mathrm{i}^{m-|m|}N_l^{|m|}P_l^{|m|}(\cos\theta)e^{\mathrm{i}m\phi}, \tag{A7}$$

with the prefactor

$$N_l^m \equiv \sqrt{\frac{2l+1}{4\pi}}\tilde{N}_l^m \equiv \sqrt{\frac{2l+1}{4\pi}\frac{(l-m)!}{(l+m)!}}. \tag{A8}$$

The factor $\mathrm{i}^{m-|m|}$ in Eq. (A7) is just a concise way of writing $(-1)^m$ if $m<0$ and $\mathrm{i}^{m-|m|} = 1$ if $m \ge 0$. Using these definitions, the coefficients in the expansion of the $Q_{12}$ kernel in spherical harmonics $Y_l^m(\theta_{12}, \phi_{12})$ are (after dividing out the normalization factor $N_l^{|m|}$)

$$\begin{aligned}
\hat{Q}_{12}^{(l,m)}/N_l^{|m|} &= \int\int \mathrm{d}\theta\mathrm{d}\phi\,\sin\theta\frac{(1-\cos\theta)}{4\pi} \\
&\quad\times[H_1 - \Delta\kappa_1\cos(2\phi)]\frac{Y_l^{m*}(\theta,\phi)}{N_l^{|m|}} \\
&= \int_{-1}^{1}\mathrm{d}z\,[P_0^0(z) - P_1^0(z)] \\
&\quad\times\left(\frac{H_1}{2}\delta_{m,0}P_l^0(z) - \frac{\Delta\kappa_1}{4}\left[\delta_{m,2} + \delta_{m,-2}\right]P_l^2(z)\right) \\
&= H_1(\delta_{l,0} - \tfrac{1}{3}\delta_{l,1})\delta_{m,0} - \tfrac{1}{4}\Delta\kappa_1\left[\delta_{m,2} + \delta_{m,-2}\right] \\
&\quad\times\int \mathrm{d}z(1-z)P_l^2(z).
\end{aligned} \tag{A9}$$

Note that the factor $\mathrm{i}^{m-|m|}$ is always equal to one here, as $m$ is always even. The integral over $z$ can be written as

$$\begin{aligned}
\int \mathrm{d}z(1-z)P_l^2(z) &= \int \mathrm{d}z(1-z)(1-z^2)\frac{d^2P_l(z)}{dz^2} \\
&= 4(-1)^l - \int \mathrm{d}z(2-6z)P_l(z) \\
&= \begin{cases} 4(-1)^l & l \ge 2, \\ 0 & l < 2, \end{cases}
\end{aligned} \tag{A10}$$

where we used partial integration, $P_0(z) = 1$ and $P_1(z) = z$ and the orthogonality of the Legendre polynomials: $\int_{-1}^{1}\mathrm{d}zP_k(z)P_l(z) = 2\delta_{k,l}/(2l+1)$.

With these expressions and Eq. (A4), we obtain

$$q_1^{(l,m)}(\mathfrak{R}) = \sum_{n=-l}^{l}\mathcal{D}^l_{mn}(\mathcal{R}_T(\mathfrak{R}))\,W_{ln}^{(1)}(\mathfrak{R}), \tag{A11}$$

where $\mathcal{D}^l_{mn}$ are the Wigner-D matrices, $\mathcal{R}_T(\mathfrak{R})$ denotes the orientation of the axis system $(\mathbf{v}_1^{\mathrm{I}}, \mathbf{v}_1^{\mathrm{II}}, \mathbf{n}_1)$ and

$$W_{ln}^{(1)}(\mathfrak{R}_1) = \begin{cases} \frac{H_1}{4\pi}\delta_{n,0} & l = 0 \\ -\frac{H_1}{4\pi}\delta_{n,0} & l = 1 \\ -(-1)^l\Delta\kappa_1 N_l^0 N_l^2[\delta_{n,2} + \delta_{n,-2}] & l \ge 2 \end{cases} \tag{A12}$$

with $H_1 = \frac{1}{2}(\kappa_1^{\mathrm{I}} + \kappa_1^{\mathrm{II}})$ the mean curvature and $\Delta\kappa_1 = \frac{1}{2}(\kappa_1^{\mathrm{I}} - \kappa_1^{\mathrm{II}})$.

Note that both $q_\alpha$ transform as the complex conjugates of the spherical harmonics do under a rotation, i.e., via the complex conjugate of Eq. (A4).

### 2. Third term in 0D-FMT: $Q_{222}$

The remaining $Q$-function, $Q_{222}$, only depends on the normal vectors $\mathbf{n}_i$ for $i$ = 1,2,3 so that it can also be expanded in spherical harmonics. The resulting expansion contains the same functions $q_2^{(l,m)}$ as for $Q_{12}$ while the constants read

$$C_{222}^{(l_1,m_1,l_2,m_2,l_3,m_3)} = \int_{(S^2)^3}\mathrm{d}\mathbf{n}^3 Q_{222}(\mathbf{n}^3)\prod_{i=1}^{3}Y_{l_i}^{m_i}(\mathbf{n}_i)N_{l_i}^0. \tag{A13}$$

We will calculate these coefficients in this section.

The explicit expression for $\alpha(\mathbf{n}_1, \mathbf{n}_2, \mathbf{n}_3)$ reads

$$\alpha(\mathbf{n}_1,\mathbf{n}_2,\mathbf{n}_3) = \arccos\left((\widehat{\mathbf{n}_1\times\mathbf{n}_2})\cdot(\widehat{\mathbf{n}_2\times\mathbf{n}_3})\right), \tag{A14}$$

where $\widehat{\mathbf{r}} = \mathbf{r}/|\mathbf{r}|$ is the direction of a vector $\mathbf{r}$. We first perform the integral $C^{(1)}(\mathbf{n}_1,\mathbf{n}_2)^{l_3}_{m_3} = 24\pi N^0_{l_3}\int\mathrm{d}\mathbf{n}_3\,Q_{222}(\mathbf{n}_1,\mathbf{n}_2,\mathbf{n}_3)\,Y^{m_3}_{l_3}(\mathbf{n}_3)$ with $8\pi\,Q_{222} = |\mathbf{n}_1\cdot(\mathbf{n}_2\times\mathbf{n}_3)|\left[\frac{2\pi}{3} - \alpha(\mathbf{n}_1,\mathbf{n}_2,\mathbf{n}_3)\right]$. Express the unit vector $\mathbf{n}_3$ in the angles $\theta$ and $\phi$ by

$$\mathbf{n}_3 = \sin\theta(\cos\phi\,\hat{b}_1 + \sin\phi\,\hat{b}_2) + \cos\theta\,\hat{b}_3, \tag{A15}$$

where $\hat{b}_2 = \widehat{\mathbf{n}_2\times\mathbf{n}_1}$, $\hat{b}_3 = \mathbf{n}_2$, and $\hat{b}_1 = \hat{b}_2\times\hat{b}_3$. As a result of the transformation (A4) of the $Y_l^m$ under a change of basis from the lab frame $\{\mathbf{e}_i\}$ to the aforementioned frame $\{\hat{b}_i\}$,

$$C^{(1)}(\mathbf{n}_1,\mathbf{n}_2)^{l_3}_{m_3} = \sum_{k=-l}^{l}\mathcal{D}_{m_3k}(\mathcal{R}_{12})C^{(2)}(\mathbf{n}_1,\mathbf{n}_2)^{l_3}_{k}, \tag{A16}$$

where $\mathcal{R}_{12}$ is the rotation defined by $\hat{b}_i = \mathcal{R}_{12}\mathbf{e}_i$ (see Eq. (A30) for an explicit expression). Here, $C^{(2)}(\mathbf{n}_1,\mathbf{n}_2)^l_m$ equals

$$N^0_{l_3}\int\int\mathrm{d}\theta\,\mathrm{d}\phi\,\sin\theta\,Q_{222}(\mathbf{n}_1,\mathbf{n}_2,\mathbf{n}_3(\theta,\phi))\,Y^m_l(\theta,\phi). \tag{A17}$$

We can simplify $\alpha(\mathbf{n}_1, \mathbf{n}_2, \mathbf{n}_3)$ by using the two equalities

$$(\widehat{\mathbf{n}_1 \times \mathbf{n}_2}) \cdot (\widehat{\mathbf{n}_2 \times \mathbf{n}_3}) = -\hat{b}_2 \cdot (\widehat{\hat{b}_3 \times \mathbf{n}_3}) = -\cos\phi, \quad \text{(A18)}$$

$$|\mathbf{n}_3 \cdot (\mathbf{n}_1 \times \mathbf{n}_2)| = |\sin\theta||\sin\phi||\mathbf{n}_1 \times \mathbf{n}_2|. \quad \text{(A19)}$$

Subsequently, we use

$$\arccos(-\cos\phi) = \pi - |\phi| \qquad \text{for } -\pi < \phi < \pi \quad \text{(A20)}$$

to write

$$\frac{C^{(2)}(\mathbf{n}_1, \mathbf{n}_2)^l_m}{|\mathbf{n}_1 \times \mathbf{n}_2|} = N^0_l \int_0^\pi \mathrm{d}\theta \int_{-\pi}^{\pi} \mathrm{d}\phi \sin^2\theta \, |\sin\phi| \times \left(|\phi| - \frac{\pi}{3}\right) Y^m_l(\theta, \phi). \quad \text{(A21)}$$

With the expression (A7) for the spherical harmonics, the integral (A21) becomes

$$C^{(2)}(\mathbf{n}_1, \mathbf{n}_2)^l_m = (2l+1)\,|\mathbf{n}_1 \times \mathbf{n}_2| I^l_m J_m \quad \text{(A22)}$$

with the following two integrals:

$$I^l_m \equiv \frac{\tilde{N}^m_l}{2} \int_0^\pi \mathrm{d}\theta \sin^2\theta \, P^m_l(\cos\theta), \quad \text{(A23)}$$

$$\begin{aligned} J_m &\equiv \frac{1}{2\pi} \int_{-\pi}^{\pi} \mathrm{d}\phi \, |\sin\phi| \left(|\phi| - \frac{\pi}{3}\right) e^{\mathrm{i}m\phi} \\ &= \int_0^\pi \mathrm{d}\phi \, \sin\phi \left(\frac{\phi}{\pi} - \frac{1}{3}\right) \cos(m\phi) \\ &= \begin{cases} -\frac{1}{4} & m = \pm 1 \\ \frac{1-2(-1)^m}{3(m^2-1)} & \text{otherwise} \end{cases}. \end{aligned} \quad \text{(A24)}$$

The symmetries of $P^m_l(\cos(\pi - \theta)) = (-1)^l P^m_l(\cos(\theta))$ under $\theta \to \pi - \theta$ cause the $l + m$ odd $\theta$ integrals to vanish and $\sin\theta = P^1_1(\cos\theta)$ and the orthogonality of the associated Legendre polynomials with equal $m$ causes the $m = \pm 1$ terms to vanish for all $l \neq 1$.

Now we calculate $I^l_m$ for even $l + m$ and $m \geq 0$, which can be simplified using

$$\sqrt{1-x^2} P^m_l(x) = \frac{1}{2l+1} \left[P^{m+1}_{l-1}(x) - P^{m+1}_{l+1}(x)\right] \quad \text{(A25)}$$

and the integral $O^m_l \equiv \int_{-1}^1 \mathrm{d}x \, P^m_l(x)$,

$$O^m_l = (-1)^m 2^{m-1} m \frac{\Gamma\left(\frac{l}{2}\right) \Gamma\left(\frac{1}{2}(m+l+1)\right)}{\Gamma\left(\frac{l+3}{2}\right) \Gamma\left(\frac{l-m+2}{2}\right)} \quad \text{(A26)}$$

for $l + m$ even and $m \leq l$, otherwise the integral is zero. Here, $\Gamma$ is the gamma function and we have used the convention $P^m_l(x) = 0$ if $m > l$. The result for $I^l_m$ is

$$I^l_m = \frac{\tilde{N}^m_l}{4l+2} \left[O^{l-1}_{m+1} - O^{l+1}_{m+1}\right]. \quad \text{(A27)}$$

The behavior of $P^m_l(x)$ under $m \to -m$ can be used to calculate $I^l_m(x) = (-1)^m I^l_{-m}(x)$ for negative $m$.

To proceed, we need the explicit form of $\mathcal{R}_{12}$ and we need to define the Wigner $D$ matrices more precisely: If $\mathcal{R}(\phi, \theta, \psi)$ is defined as

$$\mathcal{R}(\phi, \theta, \psi) = \mathcal{R}_z(\phi)\mathcal{R}_y(\theta)\mathcal{R}_z(\psi), \quad \text{(A28)}$$

where $\mathcal{R}_z$ and $\mathcal{R}_y$ denote counter-clockwise rotations around $\mathbf{e}_3$ and $\mathbf{e}_1$, respectively, then $\mathcal{D}^l_{m,n}(\mathcal{R}(\phi, \theta, \psi)) = \mathcal{D}^l_{m,n}(\phi, \theta, \psi) \equiv d^l_{m,n}(\theta) \exp(-\mathrm{i}[m\phi + n\psi]$ where $d^l_{m,n}(\theta)$ is the Wigner $d$ matrix.

Subsequently, we introduce another basis $\hat{c}_i = \mathcal{R}(\phi_2, \theta_2, 0)\mathbf{e}_i$, where $\theta_2$ and $\phi_2$ are the spherical angles of $\mathbf{n}_2$ such that $\hat{c}_3 = \mathbf{n}_2$. We express $\mathbf{n}_1$ with respect to this basis as $\mathbf{n}_1 = (\cos\phi_{12}\hat{c}_1 + \sin\phi_{12}\hat{c}_2)\sin\theta_{12} + \cos\theta_{12}\hat{c}_3$. Then

$$\mathbf{n}_2 \times \mathbf{n}_1 = (\cos\phi_{12}\hat{c}_2 - \sin\phi_{12}\hat{c}_1)\sin\theta_{12}, \quad \text{(A29)}$$

which shows that $\hat{b}_2$ can be found by a counter-clockwise rotation of $\hat{c}_2$ around $\hat{c}_3$ by an angle $-\phi_{12}$; therefore, $\hat{b}_i = \mathcal{R}(\phi_2, \theta_2, 0)\mathcal{R}_z(-\phi_{12})\mathcal{R}(\phi_2, \theta_2, 0)^{-1}\hat{c}_i = \mathcal{R}(\phi_2, \theta_2, 0)\mathcal{R}_z(-\phi_{12})\mathbf{e}_i$ for all $i$ = 1,2,3. This shows that

$$\mathcal{R}_{12} = \mathcal{R}(\phi_2, \theta_2, 0)\mathcal{R}_z(-\phi_{12}). \quad \text{(A30)}$$

Eq. (A29) also implies that $|\mathbf{n}_2 \times \mathbf{n}_1| = \sin\theta_{12}$ as $0 \leq \theta_{12} \leq \pi$.

Now we can use $\mathcal{D}^{l_3}_{m_3 p}(\mathcal{R}_{12}) = \mathcal{D}^{l_3}_{m_3 p}(\phi_2, \theta_2, -\phi_{12}) = \mathcal{D}^{l_3}_{m_3 p}(\phi_2, \theta_2, 0)\exp(\mathrm{i}p\phi_{12})$, and the transformation rule for the spherical harmonics $Y^{\mathsf{T}}_{l_1}(\mathbf{n}_1) = Y^{\mathsf{T}}_{l_1}(\theta_{12}, \phi_{12})\mathcal{D}^{l_1}(\mathcal{R}_{12})$ [see Eq. (A4)] to write

$$\begin{aligned} C^{(3)}(\mathbf{n}_2)^{l_1 l_3}_{m_1 m_3} &\equiv N^0_{l_1} \int \mathrm{d}\mathbf{n}_1 \, C^{(1)}(\mathbf{n}_1, \mathbf{n}_2)^{l_3}_{m_3} Y^{m_1}_{l_1}(\mathbf{n}_1) \\ &= \sum_{p=-l_1}^{l_1} \sum_{k=-l_3}^{l_3} \mathcal{D}^{l_1}_{m_1 k}(\phi_2, \theta_2, 0) \\ &\quad \times \mathcal{D}^{l_3}_{m_3 p}(\phi_2, \theta_2, 0) C^{(4)}_{l_1,k,p} I^{l_3}_p J_p, \end{aligned} \quad \text{(A31)}$$

where

$$\begin{aligned} C^{(4)}_{l_1,k,p} &= N^0_{l_1} \int\int \mathrm{d}\theta_{12}\mathrm{d}\phi_{12} \sin^2\theta_{12} \, e^{\mathrm{i}p\phi_{12}} Y^k_{l_1}(\theta_{12}, \phi_{12}) \\ &= \delta_{k,-p}(2l_1+1) I^{l_1}_{-p}. \end{aligned} \quad \text{(A32)}$$

The final integration over $\mathbf{n}_2$ in $C^{(\vec{l}_1, \vec{l}_2, \vec{l}_3)}_{222}$ reads

$$\begin{aligned} C^{(\vec{l}_1, \vec{l}_2, \vec{l}_3)}_{222} &= \frac{1}{8\pi} \int \mathrm{d}\mathbf{n}_2 \, C^{(3)}(\mathbf{n}_2)^{l_1 l_3}_{m_1 m_3} N^{m_2}_0 Y^{m_2}_{l_2}(\mathbf{n}_2) \\ &= C^0_{l_1 l_2 l_3} \sum_{p=-l_{13}^{\min}}^{l_{13}^{\min}} \begin{pmatrix} l_1 & l_2 & l_3 \\ m_1 & m_2 & m_3 \end{pmatrix} \begin{pmatrix} l_1 & l_2 & l_3 \\ -p & 0 & p \end{pmatrix} I^{l_1}_{-p} I^{l_3}_p J_p \\ &\equiv \begin{pmatrix} l_1 & l_2 & l_3 \\ m_1 & m_2 & m_3 \end{pmatrix} C'_{l_1 l_2 l_3}, \end{aligned} \quad \text{(A33)}$$

where $l^{\min}_{13} = \min\{l_1, l_3\}$ and $C^0_{l_1 l_2 l_3} = \frac{1}{8\pi} \prod_{i=1}^3 (2l_i + 1)$. In the first step of Eq. (A33), we used $N^0_{l_2} Y^{m_2}_{l_2}(\theta_2, \phi_2) = \frac{2l_2+1}{4\pi} \mathcal{D}^{l_2}_{m_2 0}(\phi_2, \theta_2, 0)$ and we applied the property of the Wigner $D$ matrices

$$\begin{aligned} &\int\int \sin\theta \mathrm{d}\theta\mathrm{d}\phi \, \mathcal{D}^{l_1}_{m_1,-p}(\phi, \theta, 0)\mathcal{D}^{l_2}_{m_2,0}(\phi, \theta, 0)\mathcal{D}^{l_3}_{m_3,p}(\phi, \theta, 0) \\ &= 4\pi \begin{pmatrix} l_1 & l_2 & l_3 \\ m_1 & m_2 & m_3 \end{pmatrix} \begin{pmatrix} l_1 & l_2 & l_3 \\ -p & 0 & p \end{pmatrix}, \end{aligned} \quad \text{(A34)}$$

a special case of the result from Appendix V of Brink and Satchler.[59]

The properties of $J_m$, $I^l_m$ ($I^l_m = 0$ if $l + m$ odd), and the Wigner 3-$j$ symbols cause the $C'_{l_1 l_2 l_3}$ to be zero for all $l_1$, $l_2$, and $l_3$ where $l_2$ or $l_1 + l_3$ is odd or where $l_1 \neq l_3 = 1$ or $l_3 \neq l_1 = 1$.

### 3. Third term in TR-FMT: $Q^{\mathrm{TR}}_{222}$

The coefficients $C_{\mathrm{TR}}^{(\vec{l}_1,\vec{l}_2,\vec{l}_3)}$ can be calculated similarly as above, as expression (12) reads

$$Q^{\mathrm{TR}}_{222} = \frac{1}{48\pi}[\sin\theta\sin\phi\sin\theta_{12}]^2 \tag{A35}$$

when expressed using the angles defined in Subsection 2 of the Appendix. The result has the same form as Eq. (A33) with $I^l_m$ and $J_m$ replaced by

$$(I_{\mathrm{TR}})^l_m \equiv \frac{\tilde{N}^m_l}{2}\int_0^\pi \mathrm{d}\theta\,\sin^3\theta\,P^m_l(\cos\theta) \tag{A36}$$

and

$$\begin{aligned}(J_{\mathrm{TR}})_m &\equiv \frac{1}{2\pi}\int_{-\pi}^{\pi}\mathrm{d}\phi\,\sin^2\phi\,e^{\mathrm{i}m\phi}\\ &= \frac{1}{2}\delta_{m,0} - \frac{1}{4}\left(\delta_{m,2}+\delta_{m,-2}\right),\end{aligned} \tag{A37}$$

respectively, and $C^0_{l_1l_2l_3}$ replaced by $\frac{1}{48\pi}\prod_{i=1}^3(2l_i+1)$. For $m=0$, $(I_{\mathrm{TR}})^l_m$ is easily calculated as $(1-z^2)=2(P_0(z)-P_2(z))/3$. For $m=\pm2$, we used the technique from Eq. (A10) and $\partial^2\left(1-z^2\right)^2/\partial z^2 = 4(1-3z^2) = 8P_2(z)$. Inserting these expressions in the integral of $(I_{\mathrm{TR}})^l_m$ and again applying the orthogonality of the Legendre polynomial lead to

$$(I_{\mathrm{TR}})^l_0 = \frac{2}{3}\left[\delta_{l,0} - \frac{\delta_{l,2}}{5}\right], \tag{A38}$$

$$(I_{\mathrm{TR}})^l_{\pm2} = \frac{4}{5\sqrt{6}}\delta_{l,2} \tag{A39}$$

[as $(J_{\mathrm{TR}})_m = 0$ for $m \notin \{-2,0,2\}$, the other $(I_{\mathrm{TR}})^l_m$ are not required].

### 4. Weight functions

It is common in fundamental measure theory to define weight functions (strictly speaking, most of these are distributions), which become in our case

$$w_0(\mathfrak{R}) = Q_0(\mathfrak{R})w_2(\mathfrak{R}), \tag{A40}$$

$$w^{(k)}_\alpha = q^{(k)}_\alpha w_2(\mathfrak{R}) \text{ for } \alpha = 1,2, \tag{A41}$$

$$w_3(\mathfrak{R}) = \begin{cases} 1 & \mathbf{r}\in\mathcal{B}_s(\mathbf{0},\varpi)\\ 0 & \text{otherwise}\end{cases}, \tag{A42}$$

where $w_2$ is proportional to a one-dimensional $\delta$-function such that

$$\int \mathrm{d}\mathbf{r}\,f(\mathbf{r})\,w_2(\mathbf{r},s,\varpi) = \int_{\partial\mathcal{B}_s(\mathbf{0},\varpi)} f(\mathbf{r})\,\mathrm{d}^2\mathbf{p} \tag{A43}$$

for any function $f$ (see Ref. 13 for an explicit expression for the $\delta$-function). To have a unified notation for all weight functions, we define $n^{(\vec{0})}_\alpha \equiv n_\alpha$ for $\alpha = 0, 3$ and apply similar definitions for the weight functions $w_\alpha$. With these definitions, all weighted densities have the form of Eq. 15.

## APPENDIX B: APPLICATION TO POLYHEDRA

Fundamental measure theory is formulated above for smooth particles with a well-defined, finite curvature everywhere on their surface. For polyhedra, the particles have to be smoothened by replacing the edges by cylinder sections and the vertices by spherical sections.[29] The resulting scalar weight functions $w_0$, $w_1$, $w_2$, and $w_3$ were obtained in Ref. 29 along with the vectorial and tensorial weight functions, which will be replaced by the $w^{(l,m)}_\alpha$ in this work. We start by analytically calculating the Fourier transforms (FTs) $\hat{w}^{(l,m)}_\alpha(\mathbf{k},s,\varpi)$ of the weight functions in Eqs. (A40)–(A42). Using these weight functions and the Fourier transformed density profile $\hat{\rho}(\mathbf{k},s,\varpi)$, we can efficiently calculate the weighted densities by performing an inverse Fourier transform on the FT weighted density

$$\hat{n}^{(l,m)}_\alpha(\mathbf{k}) = \sum_s \int \mathrm{d}\varpi\,\hat{w}^{(l,m)}_\alpha(\mathbf{k},s,\varpi)\,\hat{\rho}(\mathbf{k},s,\varpi), \tag{B1}$$

where we have used the convolution theorem to write the convolution in Eq. (15) as a product in Fourier space. For a polyhedron with species $s$ and orientation $\varpi$ (we suppress the dependence on $s$ and $\varpi$ for brevity), the analytical expressions for the Fourier transformed weight functions read[29]

$$\hat{w}^{(l,m)}_\alpha(\mathbf{k}) = \sum_{j=1}^{N_\alpha}\xi^{(l,m)}_{\alpha,j}\,\hat{\delta}_{\alpha,j}(\mathbf{k}), \tag{B2}$$

where we have divided the polyhedron into $N_3$ irregular tetrahedra, $\{S_{3,j}\}$, and, consequently, its surface into $N_2$ triangles, $\{S_{2,j}\}$, while $N_1$ is the number of edges, $\{S_{1,j}\}$, of the polyhedron and $N_0$ is the number of vertices, $\{S_{0,j}\}$.[47] This subdivision of the surface and interior of the particle in these simplices $S_{\alpha,j}$ allows the following closed form to be derived for the Fourier transform $\hat{\delta}_{\alpha,j}(\mathbf{k})$:

$$\begin{aligned}\hat{\delta}_{\alpha,j}(\mathbf{k}) &\equiv \int_{S_{\alpha,j}} e^{-\mathrm{i}\mathbf{k}\cdot\mathbf{r}}\mathrm{d}^\alpha\mathbf{r}\\ &= \alpha!|S_{\alpha,j}|\sum_{n=1}^{\alpha+1}\frac{\exp(-\mathrm{i}\mathbf{k}\cdot\mathbf{r}_{\alpha,j,n})}{\prod_{m=1,m\neq n}^{\alpha+1}\mathrm{i}\mathbf{k}\cdot(\mathbf{r}_{\alpha,j,m}-\mathbf{r}_{\alpha,j,n})},\end{aligned} \tag{B3}$$

where $|S_{\alpha,j}|$ is 1 for $\alpha=0$ and it is equal to the length, area, and volume of the $j$th edge, triangle, and irregular tetrahedron for $\alpha = 1$, 2, and 3, respectively, of the polyhedron. Also, the $n$th vertex of the $j$th $\alpha$-simplex is denoted by $\mathbf{r}_{\alpha,j,n}$. The $\mathbf{k}$-independent $\xi^{(l,m)}_{\alpha,j}$ consist of scalars

$$\xi^{(0,0)}_{0,j} \equiv \left[2\pi - \sum_{k=1}^{F_j}\angle_{j,k}\right]/4\pi, \tag{B4}$$

$$\xi^{(0,0)}_{1,j} \equiv \sigma_j\phi_j/8\pi, \tag{B5}$$

$$\xi^{(0,0)}_{2,j} \equiv 1, \tag{B6}$$

$$\xi^{(0,0)}_{3,j} \equiv 1, \tag{B7}$$

which are of course the same as for the previous FMT for polyhedra[29] and spherical-harmonic-like functions

$$\xi^{(l,m)}_{1,j} \equiv -\sigma_j\frac{\phi_j}{8\pi}\begin{cases}\langle\mathcal{D}^l_{m0}\rangle_j & l=1\\ N^0_lN^2_l[\langle\mathcal{D}^l_{m2}\rangle_j + \langle\mathcal{D}^l_{m2}\rangle_j] & l>1\end{cases}, \tag{B8}$$

$$\xi^{(l,m)}_{2,j} \equiv q^{(l,m)}_2 = Y^{m*}_l(\mathbf{n}_j)/N^0_l, \tag{B9}$$

where $\angle_{j,k}$ is the opening angle of face $k$ of the $F_j$ faces joined at vertex $j$, $\phi_j$ denotes the angle between the two normals, $\mathbf{n}^{\mathrm{a}}_j$

and $\mathbf{n}_j^{\mathrm{b}}$ of the faces joined in edge $j$, $\sigma_j$ is one (minus one) if the surface near edge $j$ is locally convex (concave), $\langle \mathcal{D}^l_{m0} \rangle_j$ is the average of $\mathcal{D}^l_{mn}(\mathcal{R}_T)$ over the infinitesimally thin cylinder section replacing edge $j$, and finally $\mathbf{n}_j$ is the normal of face $j$. The expressions for $\xi^{(0,0)}_{3,j}$ and $\xi^{(l,m)}_{2,j}$ can be found by simply performing the Fourier integrals in the definition of the $\hat{w}$,[29] taking into account that the normal of a face is constant. The scalar $\xi^{(0,0)}_{0,j}$ was already calculated in Ref. 29 by applying the Gauss-Bonnet theorem to the spherical section replacing the vertex to find the integrated Gaussian curvature; we will not repeat this calculation here. Finally, we will calculate $\xi^{(l,m)}_{1,j}$ in Appendix C where also the analytical expression for $\langle \mathcal{D}^l_{m0} \rangle_j$ is given.

Note that this whole calculation depends on the species $s$ and orientation $\varpi$ of the polyhedron such that it has to be repeated for every distinct polyhedral shape. However, for different orientations of the same polyhedron, $\hat{\delta}_{\alpha j}(\mathbf{k})$ only depends on the direction of $\mathbf{k}$ in the body-fixed frame of the polyhedron, while the relation $\xi^{(l,m)}_{\alpha} \to \sum_{k=-l}^{l} \mathcal{D}^l_{mk}(\mathcal{R}) \xi^{(l,k)}_{\alpha}$ under a rotation of the polyhedron by $\mathcal{R}$ can be used to avoid having to completely recalculate $\xi^{(l,m)}_{\alpha}$ for every orientation.

## APPENDIX C: CALCULATION OF THE WIGNER MATRIX AVERAGED OVER AN EDGE

As mentioned above, we replace each edge $j$ by a cylinder of radius $R$ (see the supplementary material of Ref. 29 for more details about the procedure). The cylinder section can be parametrized by an angle $\gamma$ and a coordinate $z$ along the length of the cylinder. The $\gamma$ integrals in $\xi^{(l,m)}_{j,1}$ have the form

$$\lim_{R\to 0} R \begin{Bmatrix} H_j(\mathbf{r}) \\ \Delta\kappa_j \end{Bmatrix} \int_{-\phi_j/2}^{\phi_j/2} \mathrm{d}\gamma \, \mathcal{D}^l_{mn}(\mathcal{R}_T(\gamma)), \tag{C1}$$

where the $\gamma$ dependence of $\mathcal{R}_T$ has been made explicit. The (constant) principal curvatures on the cylinder section read $\kappa^I_j = 1/R$ and $\kappa^{II}_j = 0$ such that $H_j = 1/2R$ and $\Delta\kappa_j = 1/2R$. As a result, the integral above becomes $\langle \mathcal{D}^l_{mn} \rangle_j \, \phi_j/2$ with

$$\langle \mathcal{D}^l_{mn} \rangle_j = \frac{1}{\phi_j} \int_{-\phi_j/2}^{\phi_j/2} \mathrm{d}\gamma \mathcal{D}^l_{mn}(\mathcal{R}_T(\gamma)). \tag{C2}$$

We define a basis

$$\mathbf{b}_1 = \widehat{\mathbf{n}_j^{\mathrm{a}} + \mathbf{n}_j^{\mathrm{b}}}, \tag{C3}$$

$$\mathbf{b}_2 = \widehat{\mathbf{n}_j^{\mathrm{b}} - \mathbf{n}_j^{\mathrm{a}}}, \tag{C4}$$

and

$$\mathbf{b}_3 = \widehat{\mathbf{n}_j^{\mathrm{a}} \times \mathbf{n}_j^{\mathrm{b}}} \tag{C5}$$

such that the orientation (rotation with respect to the lab frame) $\mathcal{R}_T(\gamma)$ can be written as $\mathcal{R}_j \mathcal{R}_\gamma$, where $\mathcal{R}_j$ is the orientation of the frame $\mathbf{b}_1$, $\mathbf{b}_2$, $\mathbf{b}_3$ and the rotation, $\mathcal{R}_\gamma$, has Euler angles $\psi = \pi/2$, $\theta = \pi/2$, and $\phi = \gamma$. Therefore, we can use the transformation of the Wigner-D matrix under rotations to write $\mathcal{D}^l_{mn}(\mathcal{R}_T(\gamma)) = \sum_{p=-l}^{l} \mathcal{D}^l_{mp}(\mathcal{R}_j) \mathcal{D}^l_{pn}(\mathcal{R}_\gamma)$ in Eq. (C1). Due to the choice of axes, the Wigner-D matrix $\mathcal{D}^l_{pn}(\mathcal{R}_\gamma)$ becomes $\mathcal{D}^l_{pn}(0, \pi/2, \pi/2) e^{-\mathrm{i}p\gamma}$. As a result, the average Wigner matrix becomes

$$\begin{aligned} \langle \mathcal{D}^l_{mn} \rangle_j &= \sum_{p=-l}^{l} \mathcal{D}^l_{mp}(\mathcal{R}_j) \frac{1}{\phi_j} \int_{-\phi_j/2}^{\phi_j/2} \mathrm{d}\gamma \mathcal{D}^l_{pn}(\mathcal{R}_\gamma) \\ &= \sum_{p=-l}^{l} \mathcal{D}^l_{mp}(\mathcal{R}_j) \mathcal{D}^l_{pn}(0, \pi/2, \pi/2) \mathrm{sinc}(p\phi_j/2)/2, \end{aligned} \tag{C6}$$

where $\mathrm{sinc}(x) = \sin(x)/x$.


[1] J. Gong, G. Li, and Z. Tang, Nano Today **7**, 564 (2012).
[2] L. Zhang, W. Niu, and G. Xu, Nano Today **7**, 586 (2012).
[3] Y. Xia, Y. Xiong, B. Lim, and S. Skrabalak, Angew. Chem., Int. Ed. **48**, 60 (2009).
[4] P. F. Damasceno, M. Engel, and S. C. Glotzer, Science **337**, 453 (2012).
[5] M. Dijkstra, Adv. Chem. Phys. **156**, 35 (2015).
[6] S. Torquato and Y. Jiao, Nature **460**, 876 (2009).
[7] U. Agarwal and F. A. Escobedo, Nat. Mater. **10**, 230 (2011).
[8] A. P. Gantapara, J. de Graaf, R. van Roij, and M. Dijkstra, Phys. Rev. Lett. **111**, 015501 (2013).
[9] F. Smallenburg, L. Filion, M. Marechal, and M. Dijkstra, Proc. Natl. Acad. Sci. U. S. A. **109**, 17886 (2012).
[10] R. Evans, Adv. Phys. **28**, 143 (1979).
[11] P. Tarazona, J. Cuesta, and Y. Martínez-Ratón, in *Theory and Simulation of Hard-Sphere Fluids and Related Systems*, Lecture Notes in Physics, Vol. 753, edited by Á. Mulero (Springer, Berlin, Heidelberg, 2008), pp. 247–341.
[12] H. Hansen-Goos and K. Mecke, Phys. Rev. Lett. **102**, 018302 (2009).
[13] H. Hansen-Goos and K. Mecke, J. Phys.: Condens. Matter **22**, 364107 (2010).
[14] H. Löwen, Phys. Rep. **237**, 249 (1994).
[15] P. Tarazona, Phys. Rev. Lett. **84**, 694 (2000).
[16] Y. Singh, Phys. Rep. **207**, 351 (1991).
[17] Y. Rosenfeld, Phys. Rev. Lett. **63**, 980 (1989).
[18] P. Tarazona and Y. Rosenfeld, Phys. Rev. E **55**, R4873 (1997).
[19] R. Roth, R. Evans, A. Lang, and G. Kahl, J. Phys.: Condens. Matter **14**, 12063 (2002).
[20] H. Hansen-Goos and R. Roth, J. Phys.: Condens. Matter **18**, 8413 (2006).
[21] M. Oettel, S. Görig, A. Härtel, H. Löwen, M. Radu, and T. Schilling, Phys. Rev. E **82**, 051404 (2010).
[22] A. Härtel, M. Oettel, R. E. Rozas, S. U. Egelhaaf, J. Horbach, and H. Löwen, Phys. Rev. Lett. **108**, 226101 (2012).
[23] Y. Rosenfeld, M. Schmidt, H. Löwen, and P. Tarazona, J. Phys.: Condens. Matter **8**, L577 (1996).
[24] M. Marechal, H. H. Goetzke, A. Härtel, and H. Löwen, J. Chem. Phys. **135**, 234510 (2011).
[25] A. M. Somoza and P. Tarazona, Phys. Rev. A **41**, 965 (1990).
[26] A. Poniewierski and R. Hołyst, Phys. Rev. Lett. **61**, 2461 (1988).
[27] H. Graf and H. Löwen, J. Phys.: Condens. Matter **11**, 1435 (1999).
[28] E. Velasco, L. Mederos, and D. E. Sullivan, Phys. Rev. E **62**, 3708 (2000).
[29] M. Marechal and H. Löwen, Phys. Rev. Lett. **110**, 137801 (2013).
[30] R. Wittmann, M. Marechal, and K. Mecke, J. Chem. Phys. **141**, 064103 (2014).
[31] R. Wittmann, M. Marechal, and K. Mecke, Europhys. Lett. **109**, 26003 (2015).
[32] R. Wittmann, M. Marechal, and K. Mecke, Phys. Rev. E **91**, 052501 (2015).
[33] R. Wittmann, M. Marechal, and K. Mecke, J. Phys.: Condens. Matter **28**, 244003 (2016).
[34] K. An, N. Lee, J. Park, S. C. Kim, Y. Hwang, J.-G. Park, J.-Y. Kim, J.-H. Park, M. J. Han, J. Yu, and T. Hyeon, J. Am. Chem. Soc. **128**, 9753 (2006).
[35] B. Pietrobon, M. McEachran, and V. Kitaev, ACS Nano **3**, 21 (2009).
[36] B. Wiley, Y. Sun, and Y. Xia, Acc. Chem. Res. **40**, 1067 (2007).
[37] B. S. John and F. A. Escobedo, J. Phys. Chem. B **109**, 23008 (2005).
[38] B. S. John, C. Juhlin, and F. A. Escobedo, J. Chem. Phys. **128**, 044909 (2008).
[39] Y. Rosenfeld, Phys. Rev. E **50**, R3318 (1994).
[40] The term "mixed" comes from integral geometry, see Ref. 32 for the connection.
[41] Y. Rosenfeld, M. Schmidt, H. Löwen, and P. Tarazona, Phys. Rev. E **55**, 4245 (1997).

[42]M. Marechal, S. Korden, and K. Mecke, Phys. Rev. E **90**, 042131 (2014).
[43]The functions $Q_{12}$ and $Q_{222}$ are given here in a form that is not symmetric under exchange of indices, which results in shorter expressions than the equivalent explicitly symmetric forms in Refs. 13 and 24, Appendix B.
[44]M. S. Wertheim, Mol. Phys. **83**, 519 (1994).
[45]Such an expansion can be quite easily shown to exist by an application of the Stone-Weierstrass theorem from [M. H. Stone, Math. Mag. **21**, 237 (1948)] to the subfamily of the continuous functions on $\{\partial B_s(\mathbf{0}, \varpi)\}^n$ generated by all continuous functions of the form $f_i(\mathfrak{R}^n) = f(\mathfrak{R}_i)$ for $i = 1, \ldots, n$ with $f$ any continuous function on $\{\partial B_s(\mathbf{0}, \varpi)\}$.
[46]Nevertheless, the scaling of all $z$-coordinates in the whole system (both positions and the particles themselves) by a factor $D/L$ used in Ref. 58 to study the system for $L/D \to \infty$ will also lead to strongly aligned normal vectors for any type of rod-like particle with a typical diameter $D$ and length $L$ in the limit $L/D \to \infty$. For this reason, we abandoned an approach that scaled the system to that of less elongated polyhedra. We thought initially that such an approach would allow us to use the simpler edFMT that already works well for mildly non-spherical particles, but clearly the scaling had exactly the opposite effect that we required a much more complicated theory with high truncation orders.
[47]Note that for the triangular prisms considered here, the calculation could have been optimized somewhat by taking advantage of the rectangular side faces.
[48]R. Roth, J. Phys.: Condens. Matter **22**, 063102 (2010).
[49]D. Frenkel and A. J. C. Ladd, J. Chem. Phys. **81**, 3188 (1984).
[50]L. Onsager, Ann. N. Y. Acad. Sci. **51**, 627 (1949).
[51]J. D. Parsons, Phys. Rev. A **19**, 1225 (1979).
[52]S. D. Lee, J. Chem. Phys. **87**, 4972 (1987).
[53]RAPID - Robust and Accurate Polygon Interference Detection, GAMMA Research Group at the University of North Carolina, 1997, http://gamma.cs.unc.edu/OBB/.
[54]S. Dussi and M. Dijkstra, Nat. Commun. **7**, 11175 (2016).
[55]R. van Roij, Eur. J. Phys. **26**, S57 (2005).
[56]D. Frenkel and B. Smit, *Understanding Molecular Simulation* (Academic Press, 2002).
[57]P. J. Camp and M. Allen, J. Chem. Phys. **106**, 6681 (1997).
[58]P. Bolhuis and D. Frenkel, J. Chem. Phys. **106**, 666 (1997).
[59]D. M. Brink and G. R. Satchler, *Angular Momentum*, 2nd ed. (Oxford University Press, 1968).